Materials and Design 87 (2015) 1087–1099

Contents lists available at ScienceDirect

Materials and Design

journal homepage: www.elsevier.com/locate/jmad

Modelling of the workpiece geometry effects on Ti–6Al–4V linear friction welds

Anthony R. McAndrew [a,*], Paul A. Colegrove [a], Adrian C. Addison [a], Bertrand C.D. Flipo [b], Michael J. Russell [b], Lucie A. Lee [a,b]

[a] Cranfield University, Cranfield, Bedfordshire MK43 0AL, UK
[b] TWI Ltd, Granta Park, Great Abington, Cambridge CB21 6AL, UK

ARTICLE INFO

Article history:
Received 26 May 2015
Received in revised form 6 July 2015
Accepted 15 September 2015
Available online 18 September 2015

Keywords:
Linear friction welding
Modelling
Titanium

ABSTRACT

Linear friction welding (LFW) is a solid-state joining process that is finding increasing interest from industry for the fabrication of titanium alloy (Ti–6Al–4V) preforms. Currently, the effects of the workpiece geometry on the thermal fields, material flow and interface contaminant removal during processing are not fully understood. To address this problem, two-dimensional (2D) computational models were developed using the finite element analysis (FEA) software DEFORM and validated with experiments. A key finding was that the width of the workpieces in the direction of oscillation (in-plane width) had a much greater effect on the experimental weld outputs than the cross-sectional area. According to the validated models, a decrease of the in-plane width increased the burn-off rate whilst decreasing the interface temperature, TMAZ thickness and the burn-off required to remove the interface contaminants from the weld into the flash. Furthermore, the experimental weld interface consisted of a Widmanstätten microstructure, which became finer as the in-plane width was reduced. These findings have significant, practical benefits and may aid industrialisation of the LFW process.

1. Introduction

Linear friction welding (LFW) is a solid-state joining process that works by oscillating one workpiece relative to another whilst under a large compressive force, as shown in Fig. 1(a). Despite being one continuous process, LFW is said to occur over four [1–3] phases:

- Phase 1 — initial phase. Microscopic contact exists between asperities on the two surfaces to be joined and heat is generated due to friction, see Fig. 1(b). The asperities soften and deform, increasing the true area of contact between the workpieces. Negligible axial shortening (burn-off) in the direction of the applied force is observed during this phase.
- Phase 2 — transition phase. The heat due to friction causes the interface material to plasticise and become highly viscous, as shown in Fig. 1(c). This causes the true area of contact between the workpieces to increase to 100% of the cross-sectional area. Heat conducts away from the interface, plasticising more material, and the burn-off begins to occur due to the expulsion of the viscous material from the interface.
- Phase 3 — equilibrium phase. A quasi-steady-state condition is achieved and the burn-off occurs at a nearly constant rate through the rapid generation of flash. The flash is generated in all directions — see Fig. 1(d).
- Phase 4 — deceleration phase. The relative motion is ceased and the workpieces are aligned. In some applications, an additional increased forging force may be applied to help consolidate the weld.

Components machined from solid titanium are expensive due to the large amount of material that is purchased compared to the amount that remains after machining. LFW reduces the material required to produce a component by joining smaller workpieces to produce a preform, which is subsequently machined to the desired dimensions, as shown in Fig. 2. Currently, the LFW process is an established technology for the manufacture of titanium alloy integrated bladed discs (blisks) for aero-engines [6–10]. However, due to the significant cost savings that can be achieved when fabricating components [7,8,11], LFW is finding increasing interest from other industrial sectors – particularly for the joining of Ti–6Al–4V. Despite this interest, the process has experienced limited additional industrial implementation [12,13], which is partly due to a lack of fundamental scientific understanding of LFW [13]. The rapid nature of the process and the fact that the interface of the workpieces cannot be observed during welding means that using physical experiments alone may fail to provide adequate insight into the LFW process.

Computational numerical modelling offers a pragmatic method for understanding what is happening during the rapidly evolving process [14–18]. For example, LFW models have been used to provide insight into the residual stress formation [19,20], strain rates [14,4], flash morphology [14,18,4,21], flash formation rates [14,16,17,4,21,22], thermal

* Corresponding author.
E-mail address: a.r.mcandrew@cranfield.ac.uk (A.R. McAndrew).

http://dx.doi.org/10.1016/j.matdes.2015.09.080

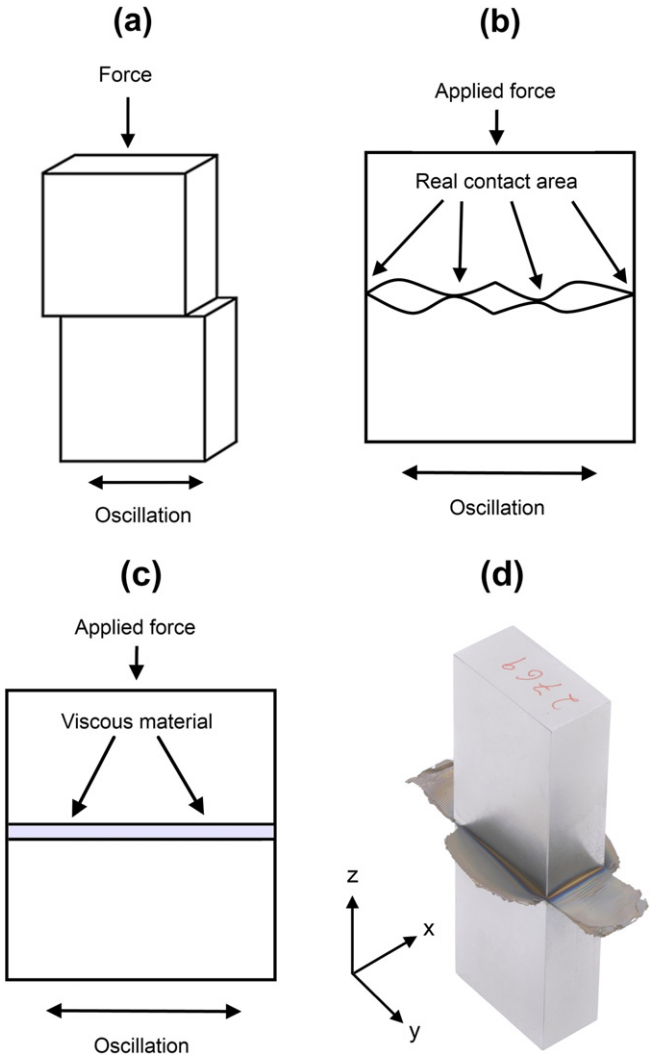

Fig. 1. (a) Illustration of the linear friction welding process, (b) asperity interaction, (c) viscous flow, and (d) a completed Ti–6Al–4V weldment showing the expelled interface material (flash) where oscillation took place in the y direction [4,5].

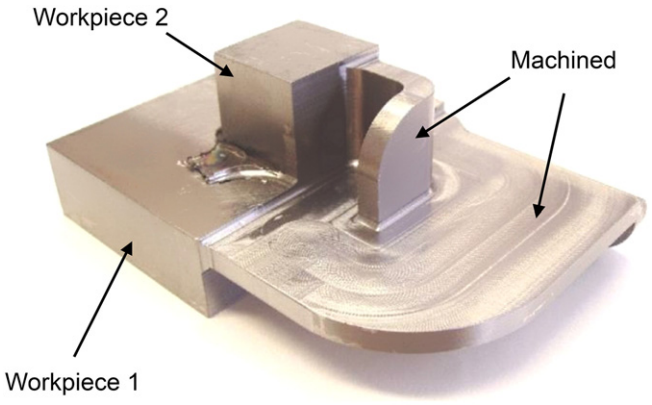

Fig. 2. Fabrication of a titanium alloy (Ti–6Al–4V) preform using the LFW process. The as-welded structure can be seen on the left side of the figure and the final machined component on the right.
Courtesy of TWI [11].

fields [3,14–17,19,4,21–27], microstructure evolution [28] and interface contaminant removal [14,4].

According to the literature, there are three primary approaches that can be used to model the LFW process. The first approach, as evidenced by the early work by Vairis and Frost [15] involved modelling only one workpiece, which was oscillated against a non-deformable surface, as illustrated in Fig. 3(a). This approach allows for quicker computational times as only half of the geometry is modelled. The problem, however, is that the coefficients of friction need to be known so that the thermal aspects of the model during phase 1 can be predicted accurately. Furthermore, due to only one workpiece being modelled, it is impossible to model the flow behaviour after the two workpieces merge to each other (see Fig. 1(c)).

As computational power increased, many authors expanded on the early approach to develop the second modelling approach, which considered both workpieces [3,16,20,22,23,26–29], as illustrated in Fig. 3(b). Many of the problems with this approach are the same as the first. For example, despite considering both workpieces, models of this type show that they never truly merge during phases 2 and 3 – as happens in reality for many materials [8,30,31] – meaning the flow behaviour after the workpieces merge to each other is still not considered.

The third approach, as shown in Fig. 3(c), was developed by Turner et al. [14], who noticed that prior to the workpieces merging there is negligible macroscopic plastic deformation, at least for the titanium alloy Ti–6Al–4V. Once a viscous layer is formed the process may be modelled as a single-body due to there being full contact between the two workpieces. A temperature profile needs to be mapped onto the single-body model to account for the heat generated prior to merging. This is vital, as the temperature profile will result in a low flow-strength for the material at the centre. This enables the material at the centre to deform in preference to the surrounding material, allowing the single body to represent two individual workpieces. Due to the merging of the interface material being modelled, this approach considers the true interface flow behaviour and produces much better replications of the flash morphology for Ti–6Al–4V workpieces [14,18,21]. The limitation of this approach is that the stages prior to workpiece merging are not modelled.

The majority of the investigations into the LFW process – modelling and experimental – have focused on characterising the "primary" process inputs, namely the amplitude, frequency, applied force/pressure and burn-off [1,5,14,4,32,33]. The effects of the workpiece geometry were often neglected. To the authors' knowledge, only two journal publications specifically comment on the geometric effects; and both were concerned with titanium alloys. Karadge et al. [9], for an identical combination of process inputs, showed that the post-weld interface grain size and the thickness of the thermo-mechanically affected zone increased when larger workpieces were used. Sorina-Müller et al. [16]

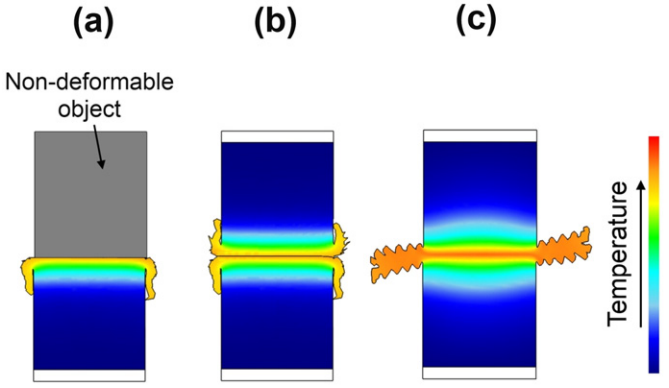

Fig. 3. Modelling approaches: (a) one workpiece, (b) two workpieces (c) a single body representing two workpieces.
Adapted from McAndrew et al. [4].

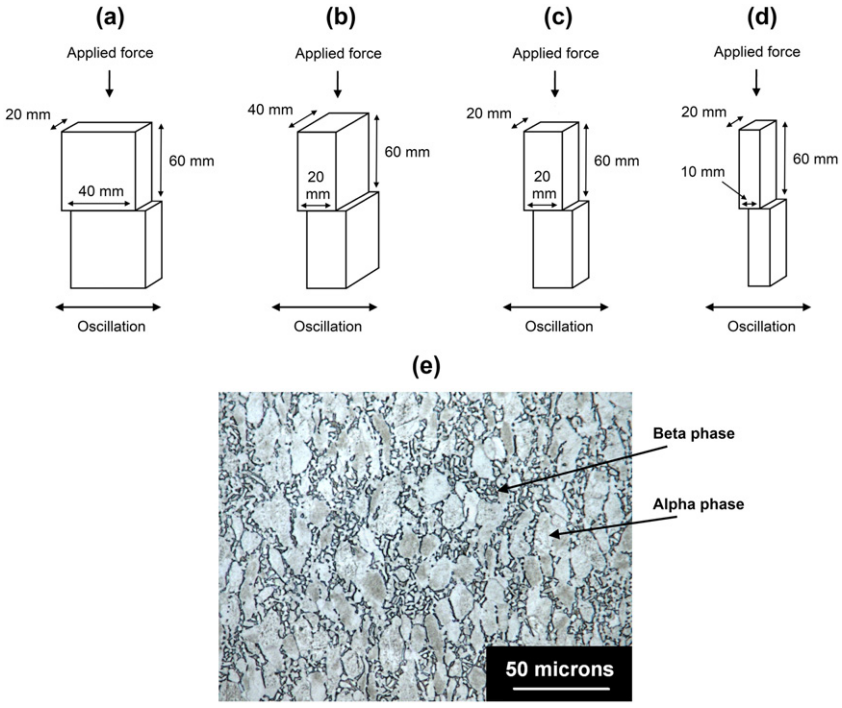

Fig. 4. (a–d) An illustration of the workpiece dimensions and directions of motion, and (e) Bi-modal alpha-beta microstructure of the material viewed under a microscope — the alpha phase microstructure is white/grey in appearance and the beta phase microstructure is black in appearance.

Table 1
Experiment conditions.

Weld	Geometry	In-plane width (mm)	Out-of-plane dimension (mm)	Cross-sectional area (mm^2)	Oscillation frequency (Hz)	Oscillation amplitude (mm)	Average rubbing velocity (mm/s)	Welding force (kN)	Welding pressure (MPa)	Burn-off (mm)
1	Fig. 4(a)	40	20	800	50	2.7	540	100	125	3
2	Fig. 4(b)	20	40	800	50	2.7	540	100	125	3
3	Fig. 4(c)	20	20	400	50	2.7	540	50	125	3
4	Fig. 4(d)	10	20	200	50	2.7	540	25	125	3

compared the interface temperatures between a “prismatic” and a “blade-like” geometry — the larger prismatic geometry had a higher peak temperature. The reasons why these phenomena occurred were not investigated in any significant detail. Furthermore, when 2D modelling Ti–6Al–4V linear friction welds, Turner et al. [14] and Schröder et al. [18,21] noticed “ripples” in the flash morphology, which was not observed by McAndrew et al. [4]. The only major difference between the models was the size of the workpieces used — the in-plane width was larger in the work by McAndrew et al. [4].

The research reported in this paper investigated the reasons why the workpiece geometry affects the process behaviour. In particular, experimentally validated 2D models were used to investigate the workpiece geometry effects on the material flow, thermal fields and interface contaminant removal during the LFW of Ti–6Al–4V workpieces.

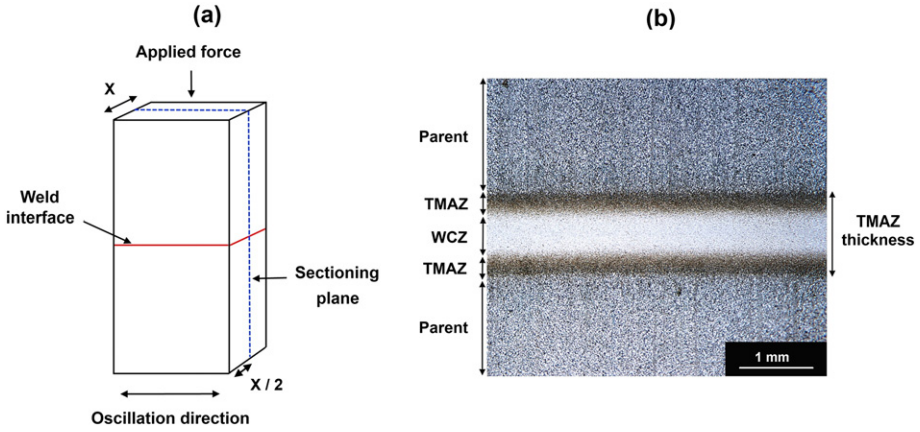

Fig. 5. (a) Location of the sectioning plane where ‘x’ represents the out-of-plane dimension, and (b) a metallographic specimen showing the weld centre zone (WCZ), thermo-mechanically affected zone (TMAZ), parent material (parent) and the TMAZ thickness [5].

Table 2
Process inputs simulated by the models.

Combination	Oscillation amplitude (mm)	Oscillation frequency (Hz)	Average rubbing velocity (mm/s)	Simulated pressure (MPa)	Burn-off (mm)
1	2.7	50	540	125	3
2	1	30	120	125	3
3	2.7	50	540	40	3
4	2	30	240	40	3

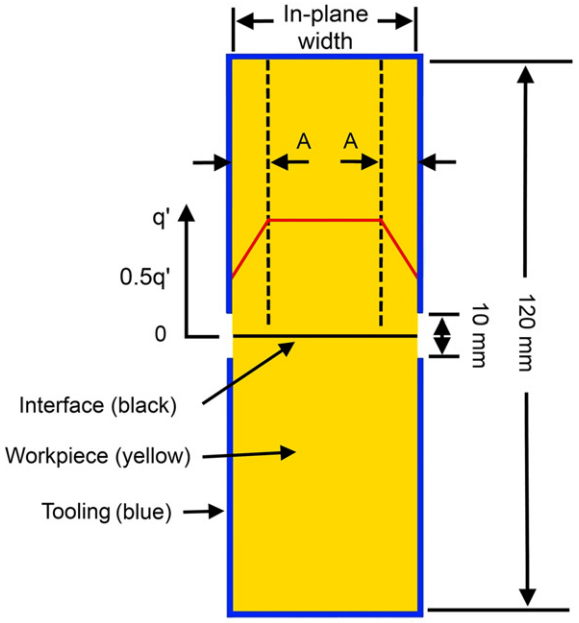

Fig. 6. Schematic diagram of the 2D thermal model. (Note that the in-plane width and the 120 mm dimension are for the workpieces only — not the tooling) [5].

2. Methodology

2.1. Experimental details

The experimental Ti–6Al–4V workpiece dimensions used in this study are displayed in Fig. 4(a–d). The Ti–6Al–4V parent material had a bimodal alpha-beta microstructure, as shown in Fig. 4(e). The experimental conditions investigated are displayed in Table 1. Note that the applied welding force was modified so that a constant normal pressure, p_n, of 125 MPa could be maintained between the different geometric conditions when the oscillatory displacement was at zero. Also listed in Table 1 is the average rubbing velocity, v_r. This term is the average absolute velocity generated over a cycle of oscillation, which Addison [11] defined as:

$$v_r = 4 \cdot A \cdot f \tag{1}$$

where: A is the oscillation amplitude and f *is* the oscillation frequency.

For the process input range investigated, McAndrew et al. [5,4] showed that the LFW outputs were primarily dependent on the average rubbing velocity. Changing the oscillation amplitude or frequency while keeping the average rubbing velocity constant only had a small impact on the results. However, it must be emphasised that this rubbing velocity phenomenon may not hold true for values outside of the amplitude (1 mm–2.7 mm) and frequency (20 Hz–70 Hz) range previously investigated by the authors [5,4] or for other materials. For each experimental condition, the forging force applied during phase 4 was kept identical to the welding force applied during the earlier phases and applied for 10 s. Worthy of note in Table 1, the in-plane width and out-of-plane dimension represent the in-plane width of the workpieces in the direction of oscillation and the dimension out-of-plane to oscillation, respectively. The welds were completed using the FW34 LFW machine (manufactured by Thompson Friction Welding) at TWI, Cambridge. The faying surfaces were cleaned with acetone immediately prior to welding.

Metallographic specimens were produced from the experiments in Table 1 in accordance with the sectioning plane shown in Fig. 5(a), i.e., they were sectioned and polished so that the centre of the weld may be viewed in-plane to the direction of oscillation. The sectioned samples were mounted and then ground using 240, 1200, 2500 and 4000 grit silicon carbide papers. After grinding, the sectioned samples were polished using colloidal silica on a micro-cloth and etched using a 3% hydrofluoric acid solution. The metallographic samples were viewed under a refractive microscope to determine the microstructure

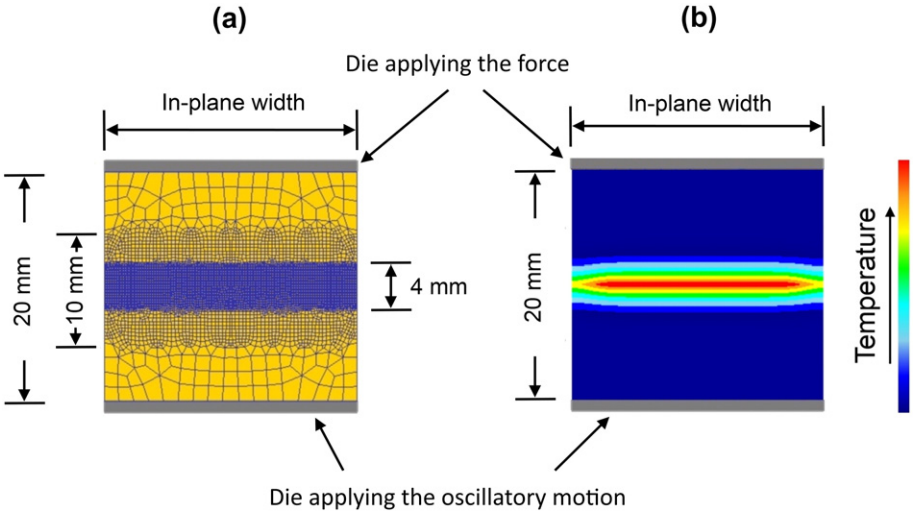

Fig. 7. (a) Example of the mesh used for the plastic flow model and (b) an illustration of the assumed phase 1 thermal profile.

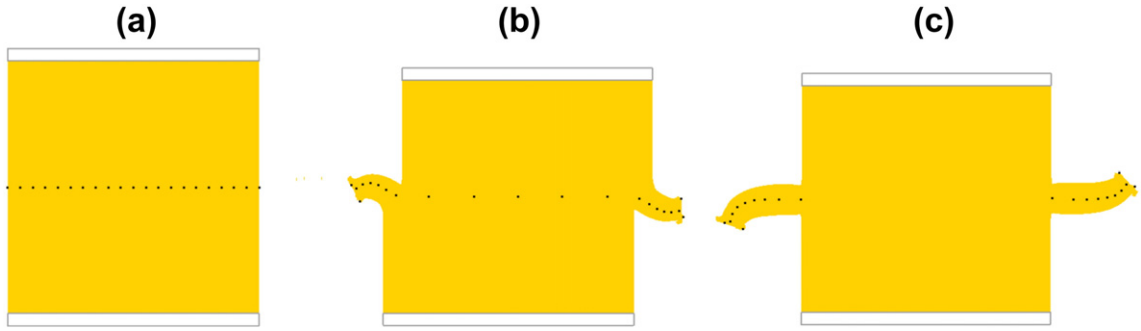

Fig. 8. Point tracking evolution: (a) initial conditions, (b) flow during processing and (c) complete expulsion.

Table 3
Experimental phase 1 responses for a rubbing velocity of 540 mm/s and a pressure of 125 MPa.

Weld	Geometry	In-plane width (mm)	Cross-sectional area (mm^2)	Average phase 1 heat flux (W/mm^2)	Average phase 1 shear stress (N/mm^2)	Phase 1 duration (s)
1	Fig. 4(a)	40	800	24.9	47.5	0.29
2	Fig. 4(b)	20	800	27.9	53.4	0.25
3	Fig. 4(c)	20	400	29.5	58.9	0.22
4	Fig. 4(d)	10	200	52.1	104.6	0.15

of the weld centre zone (WCZ) and the thermo-mechanically affected zone (TMAZ), as shown in Fig. 5(b). Technically the WCZ and the TMAZ are both "thermo-mechanically affected zones" but due to the vastly different microstructures they possess, they are often considered separately [3,7,8,30,34]. The distance from one TMAZ/parent material boundary to the other was also recorded and will be referred to as the TMAZ thickness in this publication, as shown in Fig. 5(b).

Several other responses were recorded from the experimental welds. The steady-state burn-off rate was determined by calculating the gradient of the line when the burn-off occurred at a constant rate during phase 3. In addition, the total energy input to the weld interface for a phase, E_x, was estimated [5,35] by integrating the power with respect to time:

$$E_x = \int_0^T F_{int} v \, dt \tag{2}$$

where T is the total duration of the phase, v is the velocity at a specific point in time during a sinusoidal cycle and F_{int} is the interface force at a specific point in time during a sinusoidal cycle. The experimental output data from the FW34 LFW machine was used to determine these values in accordance with the approach reported elsewhere [5,35]. To determine the *average* power input generated over a phase, the energy input for that phase was divided by the phase duration.

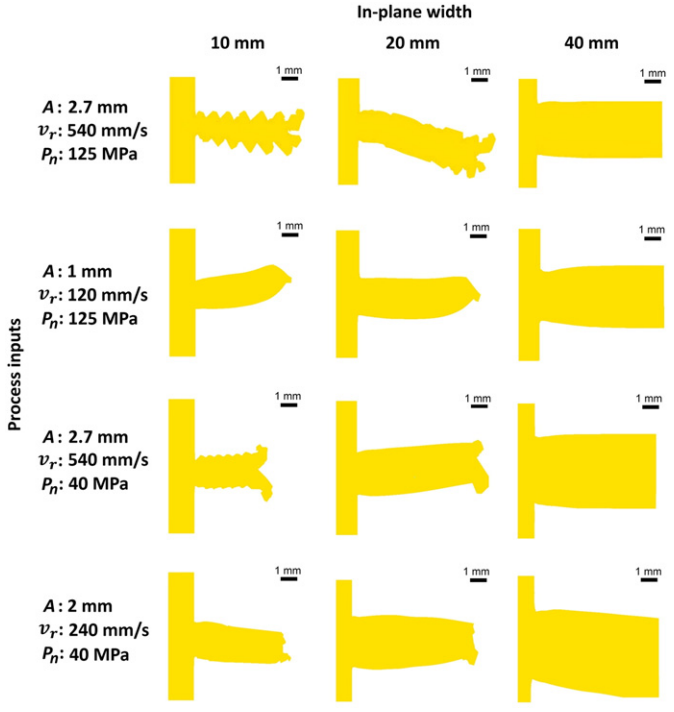

Fig. 9. FEA flash morphologies as a function of the amplitude, A; average rubbing velocity, v_r; pressure, p_n; and in-plane width. Note that not all of the flash is shown for the 40 mm cases.

2.2. Development of a model

The finite element analysis (FEA) software DEFORM was used for the modelling work. Although 2D models are unable to replicate the flash in the direction perpendicular to oscillation they still provide a good understanding of the LFW process trends [14,18,4,21,36]. Furthermore, 3D LFW process models require substantially more computational time than a 2D simulation [4], so a 2D modelling approach was used. The LFW process was represented with a 2D plane strain model that analysed a slice in the direction of oscillation at the centre of the workpieces detailed in Fig. 4(a–d). The modelling approach illustrated in Fig. 3(c) was used for the modelling work in this paper. In summary, the process was modelled as two distinct stages. The first stage used a purely thermal model to replicate the heating of the workpieces during phase 1. The second stage used a coupled thermo-mechanical plastic flow model to account for the material deformation during phases 2 and 3. The data from the phase 1 thermal model was mapped onto the plastic model to provide the initial thermal condition. The thermal and plastic models are further detailed in Sections 2.2.1 and 2.2.2, respectively.

The LFW process input combinations of interest for the modelling work are displayed in Table 2. Note that force per unit length is used to simulate the pressure in a 2D analysis. The purpose of the study was to model each process input combination detailed in Table 2 for each of the geometric conditions in Fig. 4(a–d), therefore giving 16 conditions. However, the conditions in Fig. 4(b) and (c) were suitably represented by the same 2D model — both having an in-plane width of 20 mm. This resulted in 24 models being produced, 12 thermal and 12 plastic flow.

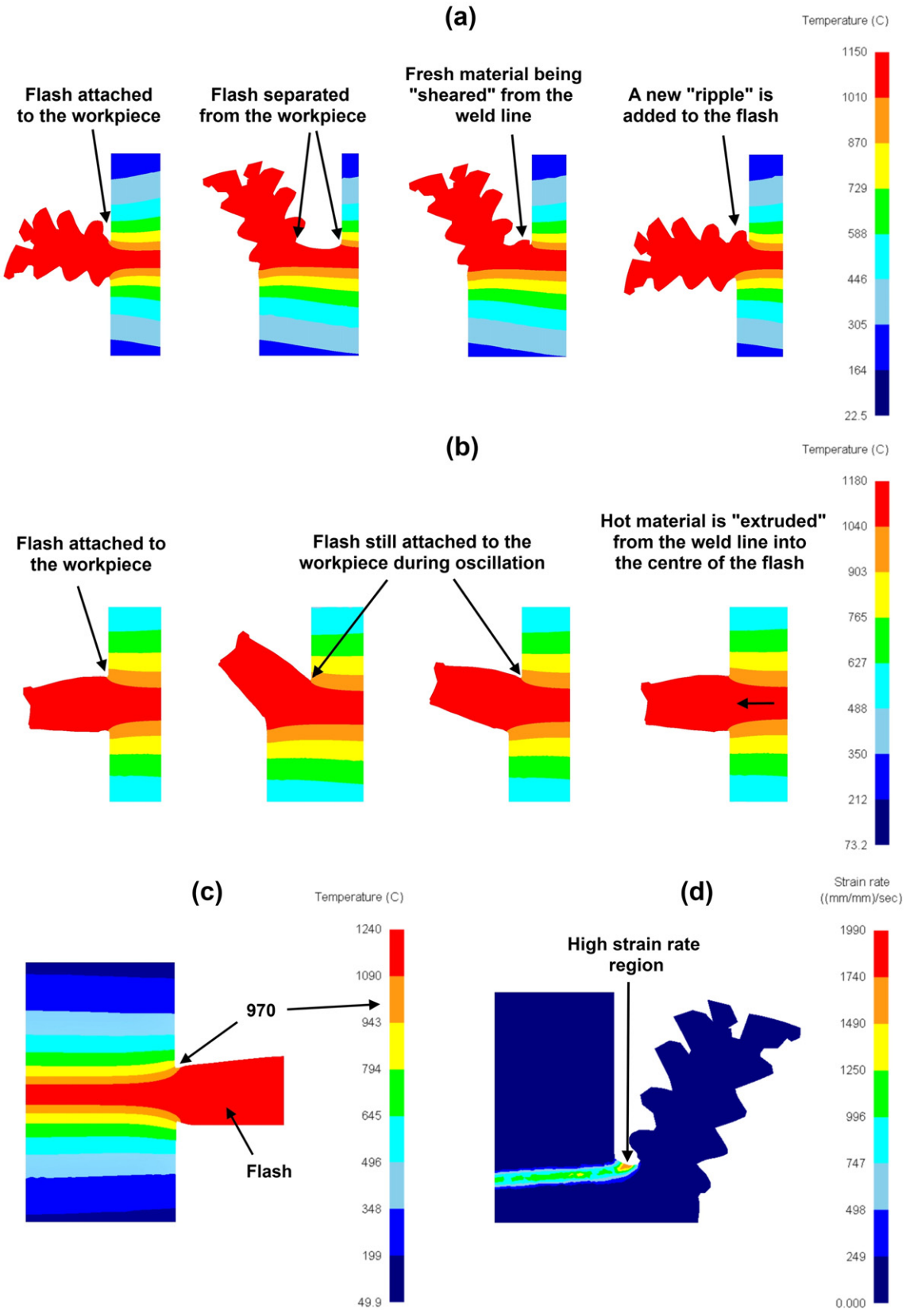

Fig. 10. Flash formation and morphology determined from the FEA, showing: (a) the mechanisms behind the ripple morphology, (b) the mechanisms behind the smooth morphology, (c) the boundary temperature between the rapidly flowing viscous material and the workpiece material with negligible flow [4] and (d) region of high strain rate.

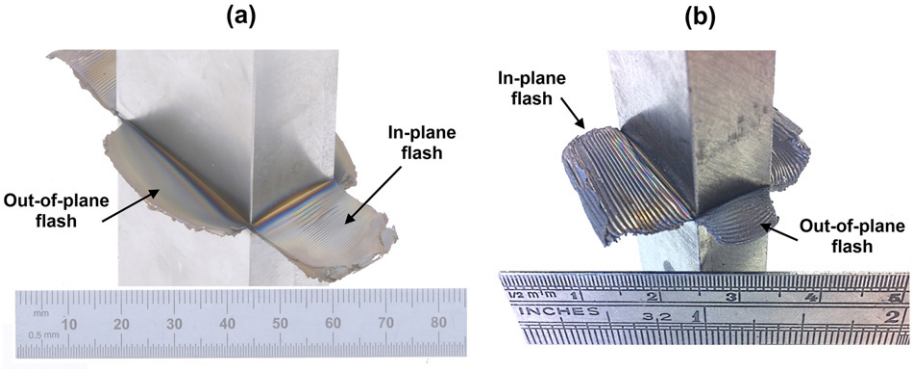

Fig. 11. Flash morphology for: (a) 40 mm in-plane width and (b) 10 mm in-plane width.

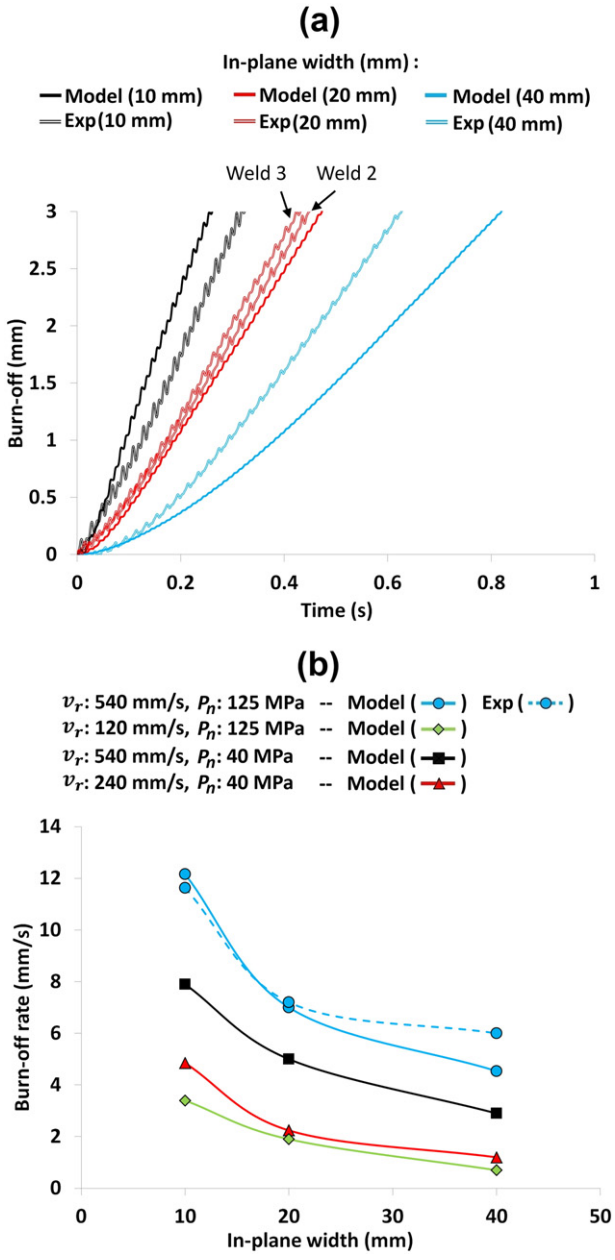

Fig. 12. A comparison of the FEA (Model) and experimental (Exp) results for: (a) the burn-off during phases 2 and 3 vs. time as a function of the in-plane width for an average rubbing velocity of 540 mm/s and a pressure of 125 MPa; and (b) burn-off rate during phase 3 as a function of the in-plane width, average rubbing velocity, v_r, and the normal pressure, p_n.

2.2.1. Thermal model (phase 1)

The 2D thermal models were developed in accordance with the dimensions shown in Fig. 6, for in-plane widths of 40 mm, 20 mm and 10 mm. A uniform mesh size of 0.5 mm was used across the thermal models. The tooling extended to within 5 mm of the interface, as it did in the experiments. Temperature dependent thermal conductivity, specific heat and emissivity data from the DEFORM software's library were used. The convective heat transfer coefficient and the conductive heat transfer coefficient with the tooling were assumed to be 10 W m^{-2} K^{-1} and 10,000 W m^{-2} K^{-1}, respectively. The temperature of the environment was assumed to be 20 °C.

A uniform heat flux (q') (W/mm^2) was applied across most of the workpiece interface which was linearly reduced to 50% of this value from the oscillation amplitude (A) away from the edge as shown in Fig. 6. The reduction at the edges was due to the sinusoidal movement of the workpieces — the point at the corner was only in contact with the other workpiece 50% of the time. The interface temperature at the end of phase 1, irrespective of the process inputs, has been shown to reach approximately 1000 °C [5], consequently, the heat flux was applied until the elements at the interface had reached this temperature. The heat flux was calculated by dividing the power input equation developed for the conditions in Fig. 4(a) by the average in-contact interface area of the workpieces over an oscillatory cycle. The power input equation was as follows [5,4]:

$$\begin{aligned}\textit{Average phase 1 power}\ (kW) = {} & -18.26366 + 0.32678 * f \\ & + 9.27832 * A + 0.061476 * F_a \\ & + 0.087638 * f * A - 4.21790 * 10^{-4} \\ & * f * F_a - 2.33759 * 10^{-3} * f^2 \\ & - 1.93524 * A^2 \end{aligned} \quad (3)$$

where: A is the oscillation amplitude (mm), f is the oscillation frequency (Hz) and F_a is the applied welding force (kN).

The heat flux was calculated for the 40 mm width case and was used for all width dimensions that used the same combination of oscillation frequency, oscillation amplitude and pressure. The validity of this approach will be discussed later in this paper.

2.2.2. Plastic flow model (phase 2 onward)

Fully coupled thermo-mechanical 2D flow models were developed for the dimensions shown in Fig. 7(a), for in-plane widths of 40 mm, 20 mm and 10 mm. The models were specifically designed to focus on the weld interface, i.e. 10 mm either side of the interface for the geometries displayed in Fig. 4(a–d) to reduce the computational time required. The temperature profile generated from the thermal model at the end of phase 1 was mapped onto the single body to account for the phase 1 heating, as illustrated in Fig. 7(b).

Since most of the plastic deformation and heat generation occurs at the interface, most of the mesh elements – with a maximum width of

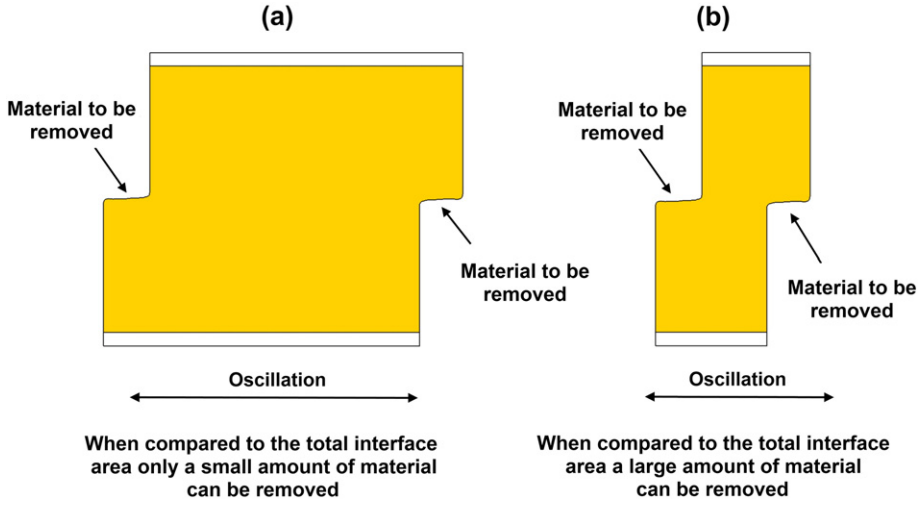

Fig. 13. Workpiece in-plane width effects on the flash formation rate for: (a) large in-plane widths and (b) small in-plane widths.

0.13 mm [4] – were placed in a 4 mm band around the interface, as shown in Fig. 7(a). The element size was increased outside of the 4 mm band. The oscillation movement and the applied force were provided by the lower and upper dies, respectively. The constitutive material data used was the same as that used by Turner et al. [14]. The material flow stress was obtained from stress and strain curves for temperatures, strains and strain rates between 20 °C and 1500 °C; 0 and 4; and 0.001 s^{-1} and 1000 s^{-1}, respectively. The values for the thermal conductivity, specific heat capacity, emissivity, and heat transfer to the tooling and environment were identical to the values used for the thermal models. Each model was given a time-step so that the oscillation movement travelled approximately one third of the interface mesh element thickness per iteration. A re-mesh was initiated every 0.1 s for all of the models. In accordance with the DEFORM user manual's recommendations [37] and other modelling work on titanium friction welding [16,17], 90% of the mechanical energy used to deform the material was estimated to be converted to heat. The remainder of the energy was assumed to be associated with causing changes in the dislocation density, grain boundary generation and migration, phase transformation and evolution, and stored in the form of crystalline defects [28,38].

Once the desired burn-off had been reached, the oscillatory and forging motions, and plastic analysis were stopped to allow the models to cool down with a time step of 0.001 s.

Several responses were recorded from the models. They included the steady-state burn-off rate, flash morphologies, thermal fields, strain rate, extent of the material being strained (FEA version of the TMAZ thickness), the average phase 3 power input and interface force, and the post oscillatory motion cooling rate. Finally, to understand the expulsion of the interface contaminants, a methodology originally proposed by Turner et al. [14], which was validated by the authors of this paper previously [4] was used. This involved placing tracked points across the interface, with a 1 mm gap between each tracked point, as shown in Fig. 8(a). The evolution of the tracked points was monitored (see Fig. 8(b)) and the amount of burn-off required to completely expel them into the flash was recorded, as shown in in Fig. 8(c). Understanding the removal of interface contaminants, such as oxides and foreign particles, is important as they can negatively affect the mechanical properties [30,39] and service life of a weld [14].

3. Results and discussion

3.1. Experimental phase one phenomena

As shown in Table 3, the experimental phase 1 heat flux, shear stress and welding duration were dependent on the workpiece geometry. As the in-plane width was decreased the heat flux and the stress increased, whilst the duration decreased. These observations can be explained by the following theory. For a constant oscillation amplitude, a reduction of the in-plane width resulted in a greater percentage of the cross-sectional area not being in-contact over an oscillatory cycle. This resulted in a greater pressure variance and hence a larger *average* pressure. For example, the average pressure over a cycle of oscillation for weld 1 and weld 4 was approximately 131 MPa and 152 MPa, respectively. Larger pressures cause more of the interface asperities to be "squashed" onto each other – particularly whilst at the end of the displacement stroke when the in-contact surface area is decreased – and require a larger force to overcome the corresponding friction [40,41]. This increased force resulted in a greater energy input (see Eq. (2).), which caused the interface material to heat and plasticise much more rapidly, thereby reducing the duration of phase 1.

There are two further observations worth commenting on. First, the difference between the heat flux, shear stress and duration values in Table 3 for welds 2 and 3 was small. This suggests that the in-plane width had a larger influence on the weld output than the overall cross sectional area (weld 2 had the same in-plane width but double the cross sectional area of weld 3). This phenomenon was also observed for a range of experimental outputs, as will be shown throughout this paper. Secondly, the values for the weld 4 heat flux and stress were almost twice as high as the other welds. This could have been a result of the greater pressure variance over a cycle of oscillation at these conditions or misaligned workpieces.

Table 4
Experimental flash measurements.

Weld	Geometry	In-plane width (mm)	Out-of-plane dimension (mm)	Ratio of in-plane to out-of plane	% of flash expelled in-plane	% of flash expelled out-of-plane
1	Fig. 4 (a)	40	20	2	53.5	46.5
2	Fig. 4 (b)	20	40	0.5	85.4	14.6
3	Fig. 4 (c)	20	20	1	79.8	20.2
4	Fig. 4 (d)	10	20	0.5	87.6	12.4

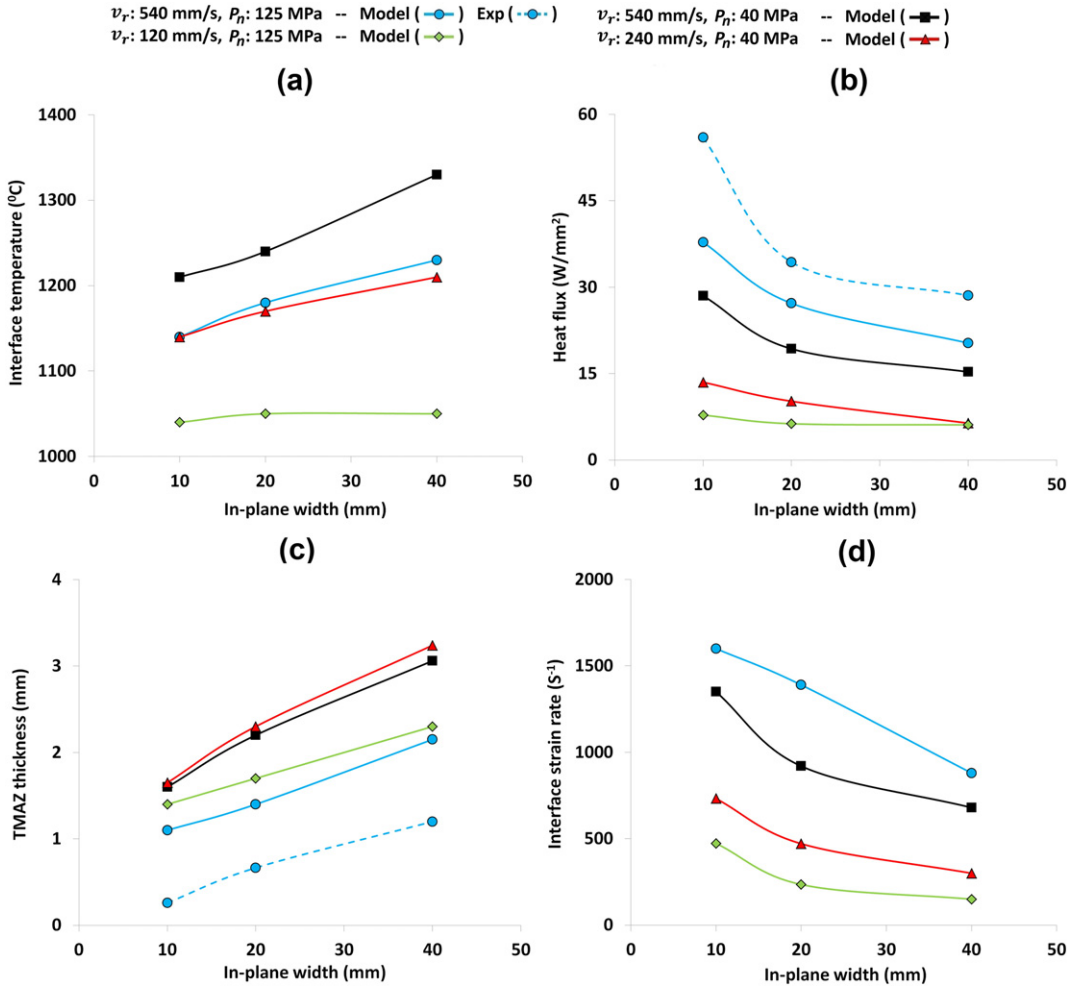

Fig. 14. FEA (model) and experimental (Exp) results as a function of average rubbing velocity, v_r, pressure, p_n, and in-plane width for the phase 3: (a) interface temperature, (b) average heat flux, (c) TMAZ thickness and (d) interface strain rate.

3.2. Material flow and thermal fields

3.2.1. Flash formation and morphology

The FEA demonstrated how the flash was generated in the direction of oscillation. When the oscillation amplitude was at maximum displacement the in-contact surface area was decreased. This caused a pressure increase, resulting in the cooler material being plunged farther into the highly viscous material. As the workpieces were brought back together, the cooler material forced the hotter viscous material from the interface. The mechanism by which the viscous material was forced from the weld was sensitive to the processing conditions simulated. Two primary flash formation mechanisms were identified, one that produced "ripples" in the flash and one that produced a "smooth" morphology, as shown in Fig. 9. The findings in Fig. 9 are in agreement with the modelling work on flash formation reported by Turner et al. [14,19] and Schröder et al. [18,21].

As originally reported by Schröder et al. [18] and supported by the present study, the ripple morphology occurred when the flash separated from the workpieces as the maximum amplitude displacement position was approached, as shown in Fig. 10(a). According to the FEA at the point of separation very high strain rates (greater than 1500 s^{-1}) were produced, see Fig. 10(d). The high strain rate regions corresponded to significant, local yielding. This phenomenon exposed a fresh layer of highly heated material, which was then sheared from the interface into the flash as the oscillatory motion was reversed. Each sheared layer corresponded to a ripple in the flash, see Fig. 10(a). In agreement with Schröder et al. [18], the FEA demonstrated that the ripples were more noticeable when the ratio between the TMAZ thickness and the oscillation amplitude was reduced. For example, as shown in Fig. 9, for a comparable amplitude, a reduction of the in-plane width or an increase of the pressure resulted in more noticeable ripples – the TMAZ thickness was reduced under these conditions. In addition, these conditions also decreased the flash thickness (see Fig. 9). Possible reasons for why the TMAZ and flash thicknesses were reduced and the strain rate increased are discussed in greater detail in Section 3.2.2. The experimental work supported the modelling findings; ripples became more defined as the in-plane width was reduced as can be seen by comparing Fig. 11(b) to Fig. 11(a). As shown in Fig. 10(b), the "smooth" morphology was produced when the flash did not separate from the workpieces. This resulted in the interface material being extruded into the centre of the flash as the oscillatory motion was reversed.

Regardless of the flash morphology type, for all cases the modelling work demonstrated that the boundary temperature between the rapidly flowing viscous material and the workpiece material with negligible flow was approximately 970 °C (±30 °C), as shown in Fig. 10(c). This is in good agreement with previous work by the authors [5,4], which showed that significant material softening occurs around the beta-transus temperature, allowing for rapid material flow. Furthermore, although the extent of highly heated material was generally constant across the in-plane width of the workpieces it increased toward the

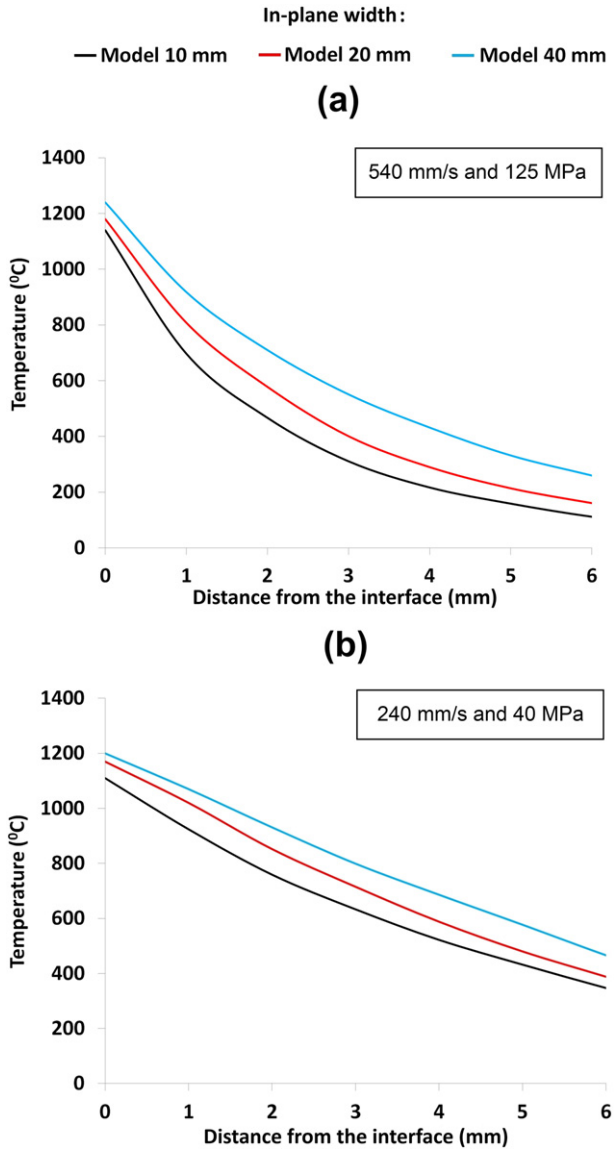

Fig. 15. FEA results for the generated phase 3 thermal profiles as a function of the in-plane width for an average rubbing velocity, v_r, and pressure, p_n, of: (a) 540 mm/s and 125 MPa and (b) 240 mm/s and 40 MPa. The thermal profiles were symmetric around the interface.

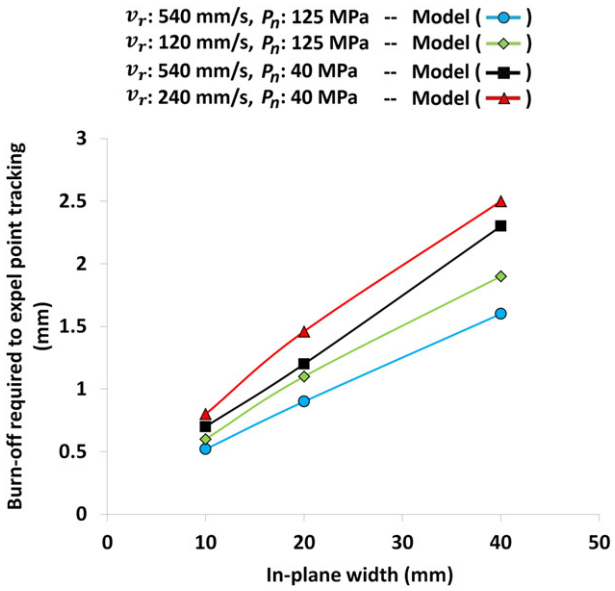

Fig. 16. FEA results for the amount of burn-off required to expel the point-tracking as a function of the in-plane width, average rubbing velocity, v_r, and pressure, p_n.

extremities of the weld – see Fig. 10(c) – possibly due to the heat from the flash conducting back into the periphery of the workpieces [24].

Fig. 12 shows the effects of the processing conditions on the rate of flash formation (burn-off rate). Note that the regression analysis graph in Fig. 12(b) – along with all other regression graphs from this point onward – present the results as a function of the average rubbing velocity. As stated previously, this was because previous work showed that changing either the amplitude or frequency whilst keeping the rubbing velocity constant had a relatively weak effect on the results for the process input range of interest in this paper [5,4].

The flash formation rate increased with an increase of the rubbing velocity or pressure, or a reduction of the in-plane width. This was due to the following: An increase of the rubbing velocity caused a faster rate of shearing/extruding; an increase of the pressure caused the cooler workpiece material to be plunged further into the viscous interface material, resulting in a greater amount of material being sheared/extruded from the interface with each oscillatory cycle; and, for a comparable set of process inputs, a reduction of the in-plane width removed a higher percentage of the total interface material with each cycle of oscillation, as shown in Fig. 13. The difference between the *experimental* 20 mm in-plane widths, i.e. experimental weld numbers 2 and 3 as illustrated in Fig. 12(a), was minimal. This further illustrates that the in-plane width has a greater overall effect on the characteristics of a weld than the total cross-sectional surface area. Consequently, an average of the burn-off rates for welds 2 and 3 was used for the 20 mm value presented in Fig. 12(b). Unless otherwise stated this approach was used for all of the experimental 20 mm in-plane width values presented in the subsequent regression graphs, i.e., an average of the experimental weld 2 and 3 values was taken due to the difference between the two individual values being minimal.

According to the results in Table 3, the assumption of a constant heat flux during phase 1 for the models that had the same rubbing velocity and pressure (see Section 2.2.1) was not fully justified. Despite this assumption, the burn-off history trends between the models and experiments were in good agreement, as shown in Fig. 12(a). This was due to the models entering phase 3 prior to any significant burn-off occurring, i.e. less than 0.5 mm. Once in phase 3, the heat generation, and therefore the thermal profiles, were dependent on the material's constitutive data. Consequently, the thermal profile used to account for the heating during phase 1 had relatively little influence on the results – Turner et al. [14] also made similar conclusions in their modelling work of Ti–6Al–4V.

In most cases, however, the 2D models under-predicted the experimental burn-off rate. This was primarily due to the 2D models not accounting for the experimental material expulsion out-of-plane to the direction of oscillation. The out-of-plane material expulsion decreased as the ratio of the in-plane width to the out-of-plane dimension was reduced, as shown in Fig. 11. In addition, the weight of the flash was measured in the in- and out-of-plane directions to oscillation for the experimental welds and the results are displayed in Table 4. Consequently, as the experimental out-of-plane material expulsion was reduced, so was the modelled under-prediction, as shown in Fig. 12. Furthermore, Table 4 also shows that there is a strong correlation between the ratio of the in-plane to the out-of-plane dimension and the percent of directional material expulsion. The 10 mm width model slightly over predicted the burn-off rate, which was probably due to either variance in the experimental results or the difference between the flow stress values in the experimental weld and the modelled weld. As shown in Fig. 12(a), the burn-off histories for all of the models did not exhibit such a defined stepwise shortening pattern when compared to a comparable experiment. This could have been due to the models not

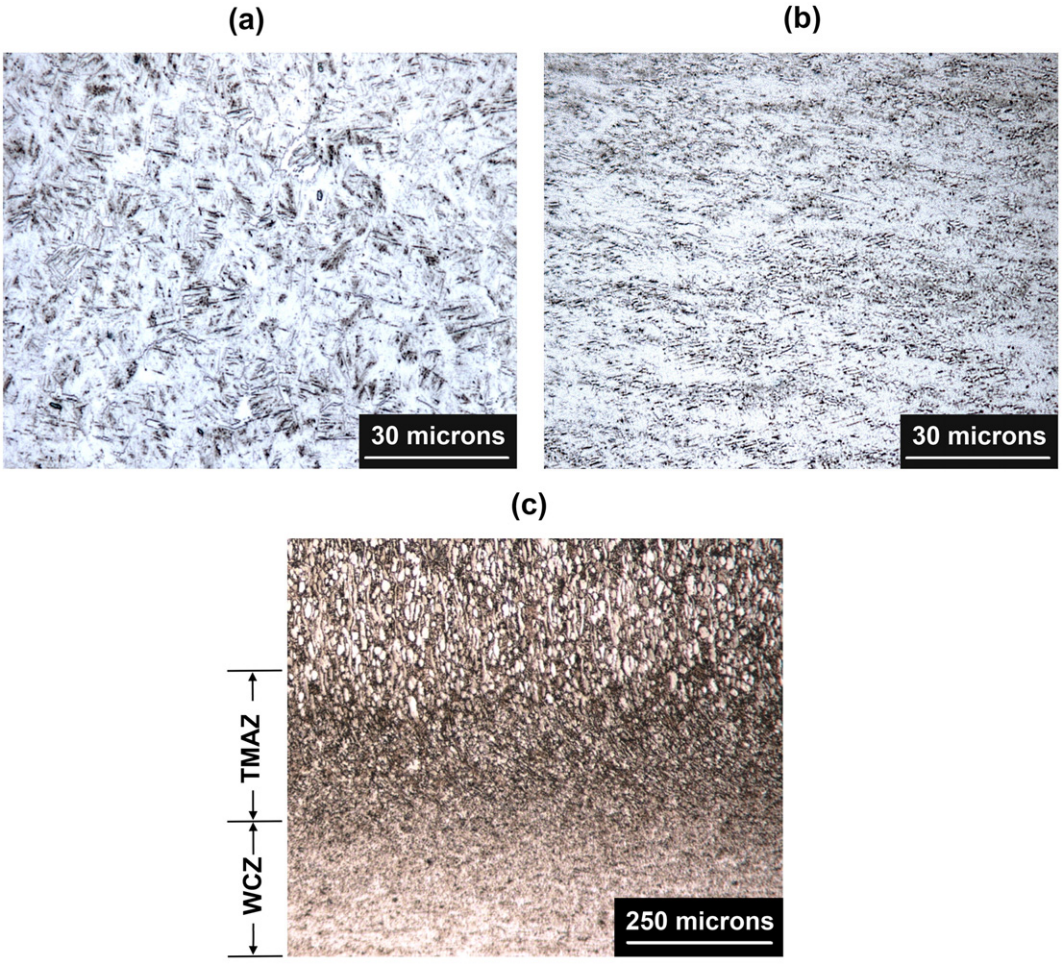

Fig. 17. Ti–6Al–4V microstructure: (a) Widmanstätten at the WCZ for weld 3 (20 mm in-plane width), (b) Widmanstätten at the WCZ for weld 4 (10 mm in-plane width) and (c) deformed, elongated and re-orientated TMAZ grains for weld 1 (40 mm in-plane width). Note that the microstructure appears finer in (b) when compared to (a).

accounting for the out-of-plane material expulsion, a misalignment of the experimental workpieces, the difference between the flow stress values, or a combination of these factors.

3.2.2. Energy, force and thermal analysis

The results for the modelled and experimental interface temperature, strain rate, average heat flux and TMAZ thickness are displayed in Fig. 14. The peak temperature and strain rate were recorded from the centre point of the interface. As shown in Fig. 14, regardless of the in-plane width, the process inputs (pressure and average rubbing velocity) had the same effect on these outputs as observed in previous work [5,4]. Consequently, they are not discussed in significant detail in this paper as the focus is on the geometry. The process input effects were as follows:

- An increase of the pressure increased the interface strain rate and heat flux, whilst decreasing the interface temperature and TMAZ thickness.
- An increase of the average rubbing velocity increased the interface temperature, strain rate and heat flux, whilst having a minimal effect on the TMAZ thickness.

As shown in Fig. 14(a), the interface temperature decreased as the in-plane width was decreased. This phenomenon might be explained by the relationship between the heat flux and the burn-off rate. For a comparable rubbing velocity and pressure, a reduction of the in-plane width increased the burn-off rate by a greater percentage than it did the heat flux, as can be seen by comparing the FEA results in Fig. 12(b) and Fig. 14(b). Although more heat per unit area went into the weld, the heat was expelled at a much faster rate. This reduced the time the heat had to conduct back from the interface causing the extent of the band of highly heated material to be reduced, see Fig. 15. Consequently, with the smaller in-plane widths, the material at a comparable point farther back from the interface was much cooler. When this cooler material reached the interface it effectively cooled the weld, producing a lower interface temperature. These findings suggest that it may be beneficial to oscillate the workpieces along the shorter of the two interface-contact dimensions. This is because the interface temperature is likely to be reduced, possibly minimising the residual stresses formed during the post oscillatory motion cooling [19,34]. The relatively cooler thermal fields for the welds that were produced with smaller in-plane widths may also be beneficial from a microstructural perspective, as will be discussed in Section 3.3.

The thinner band of highly heated material generated with the smaller in-plane widths was responsible for reducing the TMAZ thickness, as shown in Fig. 14(c). Consequently, the extent of the band of highly heated material and the TMAZ thickness are directly related. The trends for the TMAZ thickness were captured by the models, but the exact values did not match. The difference between the experimental and modelling flow stress values may have contributed to the discrepancies. The experimental welds also experienced extra material expulsion due to the forging force during phase 4, which may have reduced the experimental TMAZ values. In addition, for the models, the distance between the points of negligible strain on either side of the

interface was recorded, whereas, in the experiments, the final, observable TMAZ thickness was recorded, which may not have coincided with the points of negligible strain.

As shown in Fig. 14(b) a reduction of the in-plane width also increased the heat flux. This was believed to be due to a reduction of the interface temperature at these conditions, see Fig. 14(a). The lower interface temperature required a greater in-plane force per unit area to maintain oscillation, which increased the heat flux (see equation (2).). A possible reason for the models' under-prediction of the heat flux could have been due to the difference between the flow stress values of the experimental and the modelled welds.

As shown in Fig. 14(d), a reduction of the in-plane width also increased the peak strain rate. This was probably due to the greater force being concentrated on a smaller area of flowing material (see Fig. 14(c)). The strain rates that were recorded from the models are in closer agreement to those reported by Turner et al. [14] (500 s^{-1} to 2500 s^{-1}) and Chamanfar et al. [42] (1520 s^{-1}) to those reported by Vairis and Frost [1] (4.6 s^{-1}).

3.2.3. Interface contaminant removal

Rich and Roberts [43] suggested that the removal of the contaminants from the interface of a friction weld should not be considered as being dependent on the burn-off alone. Rather, the burn-off should be adjusted depending on the extent of flowing material/TMAZ thickness. The results from this paper support this hypothesis for the linear friction welding of Ti–6Al–4V. For example, as shown in Fig. 16, the burn-off required to remove the point tracking from the weld into the flash decreased with the in-plane width. This was due to the extent of flowing material (i.e. material above 970 °C) being reduced with smaller in-plane widths, see Fig. 15, meaning less material was required to be removed to expel the point tracking. These findings also suggest that that it may be beneficial to oscillate the workpieces along the shorter of the two interface-contact dimensions. This is because the burn-off required to remove the contaminants from the weld into the flash is likely to be reduced. Hence for the same burn-off, the factor of safety on contaminant removal is greater.

As shown in Fig. 16, the rubbing velocity had relatively little effect on the required burn-off, whilst an increase of the pressure reduced the value. This was for the same reasons reported by the authors previously [4].

3.3. Microstructure observations

The interface region of the experimental Ti–6Al–4V workpieces experienced significant microstructural changes. The welds were similar in appearance in that they had several distinct zones – a weld centre zone (WCZ), a thermo-mechanically affected zone (TMAZ) and the parent material. Due to the structural stability of Ti–6Al–4V below temperatures of 800 °C [44,45] it was often difficult to detect a purely heat affected zone. This is in good agreement with the literature [5,4,30,34,46,47].

According to the models, the WCZ of the experiments exceeded the beta-transus temperature (see Fig. 14(a)). The WCZ experienced large strains and strain rates (see Fig. 14(d)) which would have resulted in significant, dynamic recrystallisation of the high-temperature beta-phase material [48,49]. Upon cooling the recrystallised beta-phase material transformed into a Widmanstätten microstructure, as shown in Fig. 17. For the same combination of process inputs, the microstructure appeared much finer in the welds that were produced with smaller in-plane widths (compare Fig. 17(a) and (b)). This finding is in good agreement with Karadge et al. [9].

The finer microstructure for the welds produced with the smaller in-plane widths could have been due to the higher strain rates experienced (see Fig. 14(d)). This would have caused more recrystallisation during processing, refining the prior beta grains [45,49]. Furthermore, according to Gil et al. [50], the Widmanstätten morphology is finer with faster cooling rates. The modelling work showed that for an average rubbing velocity of 540 mm·s^{-1} and a pressure of 125 MPa the centre of the weld interface cooled from the beta transus temperature to 500 °C at a faster rate for the smaller in-plane widths. For example, for 40 mm, 20 mm and 10 mm in-plane widths the cooling rate was approximately 110 °C·s^{-1}, 210 °C·s^{-1} and 320 °C·s^{-1}, respectively. This phenomenon was due to the narrower band of highly heated material produced with smaller in-plane widths (see Fig. 15(a)). The narrower band of material had less heat to be conducted from the interface region into the bulk material, allowing for a faster rate of cooling. The more refined WCZ microstructure for the welds produced with the smaller in-plane widths may, according to the literature, possess superior mechanical properties [3,51,52].

Due to the original alpha-grains of the parent material being present, the material in the TMAZ did not appear to have exceeded the beta-transus temperature or experienced any noticeable dynamic recrystallisation. However, many of the TMAZ grains were deformed, elongated and re-orientated toward the direction of oscillation, as shown in Fig. 17(c), which is in agreement with the literature [5,10,4,30].

4. Conclusions

The primary conclusions from this work are as follows:

1. The 2D models captured many of the experimental weld trends and gave good insight into the LFW process for the joining of Ti–6Al–4V workpieces with different sizes.
2. For the LFW conditions evaluated, the in-plane width of the workpieces in the direction of oscillation (in-plane width) generally had a greater effect on the experimental welding process characteristics than the cross-sectional area.
3. The flash morphology was sensitive to the processing conditions. The ripple morphology became more noticeable as the ratio between the TMAZ thickness and the amplitude was reduced.
4. The experimental weld interface consisted of a Widmanstätten microstructure, which became finer when the in-plane width was reduced.
5. A reduction of the in-plane width also increased the steady-state burn-off rate, strain rate and required heat flux. Furthermore, a reduction of the in-plane width decreased the interface temperature, extent of highly heated material, TMAZ thickness and the burn-off required to remove the point tracking/interface contaminants from the weld into the flash.
6. The burn-off required to remove the interface contaminants into the flash should not be considered as a stand-alone value, but rather as a function of the generated TMAZ thickness. As the TMAZ thickness is increased more burn-off is required to expel the interface contaminants. These findings suggest that it may be beneficial to oscillate the workpieces along the shorter of the two interface-contact dimensions. This is because the burn-off required to remove the interface contaminants into the flash is likely to be reduced. Hence, for the same burn-off, the factor of safety on contaminant removal is greater. Furthermore, these conditions are also likely to decrease the interface temperature, which may offer additional process benefits.

Acknowledgements

The authors would like to thank the Engineering and Physical Sciences Research Council (EPSRC), The Boeing Company and The Welding Institute (TWI) for funding the research presented in this paper. Also, the advice provided by Dr. Filomeno Martina of Cranfield University was greatly appreciated.

Enquiries for access to the data referred to in this article should be directed to researchdata@cranfield.ac.uk.

References

[1] A. Vairis, M. Frost, High frequency linear friction welding of a titanium alloy, Wear 217 (1998) 117–131.
[2] A. Vairis, M. Frost, On the extrusion stage of linear friction welding of Ti–6Al–4V, Mater. Sci. Eng. A 271 (1999) 477–484.
[3] M. Grujicic, G. Arakere, B. Pandurangan, C.F. Yen, B.A. Cheeseman, Process modeling of Ti–6Al–4V linear friction welding (LFW), J. Mater. Eng. Perform. 21 (2011) 2011–2023.
[4] A.R. McAndrew, P.A. Colegrove, A.C. Addison, B.C.D. Flipo, M.J. Russell, Modelling the influence of the process inputs on the removal of surface contaminants from Ti–6Al–4V linear friction welds, Mater. Des. 66 (2015) 183–195.
[5] A.R. McAndrew, P.A. Colegrove, A.C. Addison, B.C.D. Flipo, M.J. Russell, Energy and force analysis of Ti–6Al–4V linear friction welds for computational modeling input and validation data, Metall Mater Trans A 45 (2014) 6118–6128.
[6] Y. Guo, T. Jung, Y. Lung, H. Li, S. Bray, P. Bowen, Microstructure and microhardness of Ti6246 linear friction weld, Mater. Sci. Eng. A 562 (2013) 17–24.
[7] I. Bhamji, M. Preuss, P.L. Threadgill, A.C. Addison, Solid state joining of metals by linear friction welding: a literature review, Mater. Sci. Technol. 27 (2011) 2–12.
[8] A.C. Addison, Linear friction welding of engineering metals, TWI industrial members report — 894/2008, Cambridge, U.K., 2008.
[9] M. Karadge, M. Preuss, C. Lovell, P.J. Withers, S. Bray, Texture development in Ti–6Al–4V linear friction welds, Mater. Sci. Eng. A 459 (2007) 182–191.
[10] Y. Guo, Y. Chiu, M. Attallah, H. Li, Characterization of dissimilar linear friction welds of alpha + beta titanium alloys, J. Mater. Eng. Perform. 21 (2012) 770–776.
[11] A.C. Addison, Linear friction welding information for production engineering, TWI industrial members report — 961/2010, Cambridge, U.K., 2010.
[12] A.M.M. García, BLISK fabrication by linear friction welding, in: E. Benini (Ed.), Adv. Gas Turbine Technol. InTech, Winchester 2011, pp. 411–434.
[13] W. Li, J. Suo, T. Ma, Y. Feng, K. Kim, Abnormal microstructure in the weld zone of linear friction welded Ti–6.5Al–3.5Mo–1.5Zr–0.3Si titanium alloy joint and its influence on joint properties, Mater. Sci. Eng. A 599 (2014) 38–45.
[14] R. Turner, J.-C. Gebelin, R.M. Ward, R.C. Reed, Linear friction welding of Ti–6Al–4V: modelling and validation, Acta Mater. 59 (2011) 3792–3803.
[15] A. Vairis, M. Frost, Modelling the linear friction welding of titanium blocks, Mater. Sci. Eng. A 292 (2000) 8–17.
[16] J. Sorina-Müller, M. Rettenmayr, D. Schneefeld, O. Roder, W. Fried, FEM simulation of the linear friction welding of titanium alloys, Comput. Mater. Sci. 48 (2010) 749–758.
[17] W. Li, T. Ma, J. Li, Numerical simulation of linear friction welding of titanium alloy: effects of processing parameters, Mater. Des. 31 (2010) 1497–1507.
[18] F. Schröder, R.M. Ward, A.R. Walpole, R.P. Turner, M.M. Attallah, J.-C. Gebelin, et al., Linear friction welding of Ti6Al4V: experiments and modelling, Mater. Sci. Technol. 31 (2015) 372–384.
[19] R. Turner, R.M. Ward, R. March, R.C. Reed, The magnitude and origin of residual stress in Ti–6Al–4V linear friction welds: an investigation by validated numerical modeling, Metall. Mater. Trans. B Process Metall. Mater. Process. Sci. 43 (2012) 186–197.
[20] X. Song, M. Xie, F. Hofmann, T.S. Jun, T. Connolley, C. Reinhard, et al., Residual stresses in linear friction welding of aluminium alloys, Mater. Des. 50 (2013) 360–369.
[21] F. Schroeder, R.M. Ward, R.P. Turner, M.M. Attallah, J. Gebelin, R.C. Reed, Linear friction welding of titanium alloys for aeroengine applications: modelling and validation, . 9th Int. ConfTrends Weld. Res., Chicago, U.S.A., 2012 886–892.
[22] E. Ceretti, L. Fratini, C. Giardini, D. Spisa, Numerical modelling of the linear friction welding process, Int. J. Mater. Form. 3 (2010) 1015–1018.
[23] L. Fratini, G. Buffa, D. Campanella, D. La Spisa, Investigations on the linear friction welding process through numerical simulations and experiments, Mater. Des. 40 (2012) 285–291.
[24] W. Li, S.X. Shi, F.F. Wang, T.J. Ma, J.L. Li, D.L. Gao, et al., Heat reflux in flash and its effect on joint temperature history during linear friction welding of steel, Int. J. Therm. Sci. 67 (2013) 192–199.
[25] J. Tao, T. Zhang, P. Liu, J. Li, Y. Mang, Numerical computation of a linear friction welding process, Mater Sci Forum 575–578 (2008) 811–815.
[26] X. Wu, Finite element simulation of linear friction welding, Adv. Mater. Res. 411 (2012) 126–129.
[27] A.T. Bikmeyev, R.K. Gazizov, A. Vairis, A.M. Yamileva, Modelling the temperature distribution in the contact area of a moving object in the case of linear friction welding, Proc. ASME 2013 Int. Mech. Eng. Congr. Expo. IMECE2013, ASME, San Diego, California, U.S.A. 2013, pp. 1–8.
[28] M. Grujicic, R. Yavari, J.S. Snipes, S. Ramaswami, C.-F. Yen, B.A. Cheeseman, Linear friction welding process model for carpenter custom 465 precipitation-hardened martensitic stainless steel, J. Mater. Eng. Perform. 23 (2014) 2182–2198.
[29] M. Vaziri, S. Berg, D. Sandberg, I.T. Gheinani, Three-dimensional finite element modelling of heat transfer for linear friction welding of scots pine, Wood Mater. Sci Eng. 1–8 (2014).
[30] P. Wanjara, M. Jahazi, Linear friction welding of Ti–6Al–4V: processing, microstructure, and mechanical-property inter-relationships, Metall Mater Trans A 36 (2005) 2149–2164.
[31] B. Lang, T.C. Zhang, X.H. Li, D.L. Guo, Microstructural evolution of a TC11 titanium alloy during linear friction welding, J. Mater. Sci. 45 (2010) 6218–6224.
[32] A. Chamanfar, M. Jahazi, J. Gholipour, P. Wanjara, S. Yue, Mechanical property and microstructure of linear friction welded waspaloy, Metall Mater Trans A 42 (2010) 729–744.
[33] T.-S. Jun, F. Rotundo, X. Song, L. Ceschini, A.M. Korsunsky, Residual strains in AA2024/AlSiCp composite linear friction welds, Mater. Des. 31 (2010) S117–S120.
[34] J. Romero, M.M. Attallah, M. Preuss, M. Karadge, S.E. Bray, Effect of the forging pressure on the microstructure and residual stress development in Ti–6Al–4V linear friction welds, Acta Mater. 57 (2009) 5582–5592.
[35] U.U. Ofem, P.A. Colegrove, A. Addison, M.J. Russell, Energy and force analysis of linear friction welds in medium carbon steel, Sci. Technol. Weld. Join. 15 (2010) 479–485.
[36] Turner R, Schroeder F, Ward RM, Brooks JW. The importance of materials data and modelling parameters in an FE simulation of linear friction welding. Adv. Mater. Sci. Eng. 2014;2014:1–8.
[37] Scientific Forming Technologies Corporation (SFTC), DEFORM User's Manual V.11(Columbus, Ohio, USA) 2014.
[38] H. Pashazadeh, J. Teimournezhad, A. Masoumi, Numerical investigation on the mechanical, thermal, metallurgical and material flow characteristics in friction stir welding of copper sheets with experimental verification, Mater. Des. 55 (2014) 619–632.
[39] A. Chamanfar, M. Jahazi, J. Gholipour, P. Wanjara, S. Yue, Maximizing the integrity of linear friction welded waspaloy, Mater. Sci. Eng. A 555 (2012) 117–130.
[40] B. Bhushan, Introduction to Tribology, 2nd ed. New York, NY, John Wiley and Sons, inc, 2002.
[41] F.P. Bowden, D. Tabor, The Friction and Lubrication of Solids, Oxford University Press, London, England, 1950.
[42] A. Chamanfar, M. Jahazi, J. Gholipour, P. Wanjara, S. Yue, Modeling grain size and strain rate in linear friction welded waspaloy, Metall Mater Trans A 44 (2013) 4230–4238.
[43] T. Rich, R. Robert, The forge phase of friction welding, Weld. J. 53 (1971) 137–146.
[44] T.J. Ma, W.-Y. Li, Q.Z. Xu, Y. Zhang, J.L. Li, S.Q. Yang, et al., Microstructure evolution and mechanical properties of linear friction welded 45 steel joint, Adv. Eng. Mater. 9 (2007) 703–707.
[45] T. Seshacharyulu, S.C. Medeiros, W.G. Frazier, Y.V.R.K. Prasad, Hot working of commercial Ti–6Al–4V with an equiaxed alpha-beta microstructure: materials modeling considerations, Mater. Sci. Eng. A 284 (2000) 184–194.
[46] W. Li, T. Ma, Y. Zhang, Q. Xu, J. Li, S. Yang, et al., Microstructure characterization and mechanical properties of linear friction welded Ti–6Al–4V alloy, Adv. Eng. Mater. 10 (2008) 89–92.
[47] T.J. Ma, W.-Y. Li, S.Y. Yang, Impact toughness and fracture analysis of linear friction welded Ti–6Al–4V alloy joints, Mater. Des. 30 (2009) 2128–2132.
[48] R. Ding, Z.X. Guo, A. Wilson, Microstructural evolution of a Ti–6Al–4V alloy during thermomechanical processing, Mater. Sci. Eng. A 327 (2002) 233–245.
[49] T. Seshacharyulu, S.C. Medeiros, W.G. Frazier, Y.V.R.K. Prasad, Microstructural mechanisms during hot working of commercial grade Ti–6Al–4V with lamellar starting structure, Mater. Sci. Eng. A 325 (2002) 112–125.
[50] F.J. Gil, M.P. Ginebra, J.M. Manero, J.A. Planell, Formation of alpha-Widmanstatten structure: effects of grain size and cooling rate on the Widmanstatten morphologies and on the mechanical properties in Ti6Al4V alloy, J. Alloys Compd. 329 (2001) 142–152.
[51] Y. Zhang, Y.S. Sato, H. Kokawa, S.H.C. Park, S. Hirano, Microstructural characteristics and mechanical properties of Ti–6Al–4V friction stir welds, Mater. Sci. Eng. A 485 (2008) 448–455.
[52] G. Lütjering, Influence of processing on microstructure and mechanical properties of (alpha + beta) titanium alloys, J. Alloys Compd. 243 (1998) 32–45.